Optical forces and torques on realistic plasmonic nanostructures: a surface integral approach

Alok Ji,[1,2,†] T. V. Raziman,[1,†] Jérémy Butet,[1] R. P. Sharma,[2] and Olivier J. F. Martin[1,*]

[1]*Nanophotonics and Metrology Laboratory (NAM), Swiss Federal Institute of Technology Lausanne (EPFL), Switzerland*

[2]*Centre for Energy Studies, Indian Institute of Technology Delhi, India*

**Corresponding author: olivier.martin@epfl.ch*

Received May 30, 2014; accepted July 3, 2014;
posted July 9, 2014 (Doc. ID 213164); published August 6, 2014

We develop a novel formalism to calculate the optical forces and torques on complex and realistic nanostructures by combining the surface integral equation (SIE) technique with Maxwell's stress tensor. The optical force is calculated directly on the scatterer surface from the currents obtained from the SIE, which does not require an additional surface to evaluate Maxwell's stress tensor; this is especially useful for intricate geometries such as plasmonic antennas. SIE enables direct evaluation of forces from the surface currents very efficiently and accurately for complex systems. As a proof of concept, we establish the accuracy of the model by comparing the results with the calculations from the Mie theory. The flexibility of the method is demonstrated by simulating a realistic plasmonic system with intricate geometry.

OCIS codes: (350.4855) Optical tweezers or optical manipulation; (240.6680) Surface plasmons; (250.5403) Plasmonics.

http://dx.doi.org/10.1364/OL.39.004699

Optical forces find numerous applications in various areas of physical and life sciences [1–3]. Recently, the utilization of complex optical landscapes, such as those produced by nanostructures—in particular plasmonic nanostructures—has opened new possibilities for trapping and manipulating structures at the nanoscale using near-field optical forces [4–10].

In the light of present and forthcoming opportunities to exploit optical forces, there is a need for versatile numerical techniques with the ability to simulate optical forces and torques on complicated systems with intricate geometries. Different approaches can be used to compute optical forces, including interacting dipoles [11–14], an analytical two spheres model [15], a generalized Mie approach, [16], and numerical approaches using finite difference time domain [17].

To analyze optical forces on realistically shaped structures, we need to use numerical techniques since no analytical methods are available for such general calculations [18]. The Maxwell's stress tensor is used to calculate the forces on materials with a boundary S. The conservation of momentum for the present case is written as [19]:

$$\frac{\partial(\mathbf{P}_{\text{mech}}+\mathbf{P}_{\text{field}})_i}{\partial t}=\oint_S\sum_j\sigma_{ij}n_j\mathrm{d}S, \tag{1}$$

where $\mathbf{P}_{\text{mech}}$ and $\mathbf{P}_{\text{field}}$ are the mechanical and electromagnetic momenta, respectively. The vector $\hat{\mathbf{n}}$ is the outward normal to the closed surface S, and σ is the Maxwell's stress tensor with components given by:

$$\sigma_{ij}=\epsilon_0\epsilon E_iE_j+\mu_0\mu H_iH_j-\frac{1}{2}(\epsilon_0\epsilon E_kE_k+\mu_0\mu H_kH_k)\delta_{ij}, \tag{2}$$

where ϵ and μ are the relative permittivity and relative permeability of the background, respectively. If the fields have harmonic dependence ($e^{-i\omega t}$), the time average of the stress tensor over a cycle can be written as

$$\langle\sigma_{ij}\rangle=\frac{1}{2}\Re[\epsilon_0\epsilon E_iE_j^*+\mu_0\mu H_iH_j^*-\frac{1}{2}(\epsilon_0\epsilon E_kE_k^*+\mu_0\mu H_kH_k^*)\delta_{ij}]. \tag{3}$$

The time average of $\mathbf{P}_{\text{field}}$ over an entire period is a constant. Hence, its derivative vanishes and the left hand side of Eq. (1) reduces to the total force on the volume enclosed by S. Thus the time averaged optical force acting on the material is given by [20]:

$$\langle F_i\rangle=\oint_S\langle\sigma_{ij}\rangle n_j\mathrm{d}S. \tag{4}$$

The commonly used method to calculate optical forces from Eq. (4), illustrated in Fig. 1(a), is to choose a large number of points on a surface enclosing the particle and perform numerical integration of the Maxwell's stress tensor over these points. This method has a few drawbacks. First, achieving sufficient numerical accuracy requires the evaluation of fields at a large number of points on the surface, which is computationally expensive. In addition, it is not always easy to generate points over a surface enclosing only the particle when the particle is placed in lossy media or in the vicinity of some other nanostructure [21].

To overcome these difficulties, we utilize the surface integral equation (SIE) formulation for the light scattering simulations. SIE is related to boundary element methods [22,23] and uses the Green's tensor method to simulate light interaction with matter accurately and efficiently. The SIE code developed here can simulate scattering from multiple nanostructures [24] as well as periodic nanostructure arrays [25]. The outputs of SIE simulations are electric and magnetic currents over the triangular surface mesh elements. We evaluate the Maxwell's stress tensor and hence the force over the surface mesh directly from these currents, as illustrated in Fig. 1(b). There is no intermediate computation of

electric and magnetic fields, thereby improving both the accuracy and the speed of calculation. Furthermore, no imaginary surface needs to be generated around the particle and the method is able to deal with particles placed very close to each other as well. Since we have discretized our surface into triangles, the total optical force acting on the object will be

$$\langle F_i \rangle = \sum_T \int_T \langle \sigma_{ij} \rangle n_j \mathrm{d}S_T, \tag{5}$$

where T is the triangles on the surface of the object. SIE defines the electric and magnetic surface currents as

$$\mathbf{J} = \hat{\mathbf{n}} \times \mathbf{H}, \tag{6}$$

$$\mathbf{M} = -\hat{\mathbf{n}} \times \mathbf{E}. \tag{7}$$

The parallel components of the fields ($\mathbf{E}_\parallel$ and $\mathbf{H}_\parallel$) can be expressed directly in terms of surface currents:

$$\mathbf{H}_\parallel = \mathbf{J} \times \hat{\mathbf{n}}, \tag{8}$$

$$\mathbf{E}_\parallel = \hat{\mathbf{n}} \times \mathbf{M}. \tag{9}$$

We can use Maxwell's equations to derive the perpendicular components of the fields ($\mathbf{E}_\perp$ and $\mathbf{H}_\perp$) from the surface currents:

$$\mathbf{E}_\perp = -\frac{i}{\omega\epsilon}(\nabla \cdot \mathbf{J})\hat{\mathbf{n}}, \tag{10}$$

$$\mathbf{H}_\perp = -\frac{i}{\omega\mu}(\nabla \cdot \mathbf{M})\hat{\mathbf{n}}. \tag{11}$$

Combining these results, we obtain the surface fields entirely in terms of the surface currents:

$$\mathbf{E} = -\frac{i}{\omega\epsilon}(\nabla \cdot \mathbf{J})\hat{\mathbf{n}} + \hat{\mathbf{n}} \times \mathbf{M}, \tag{12}$$

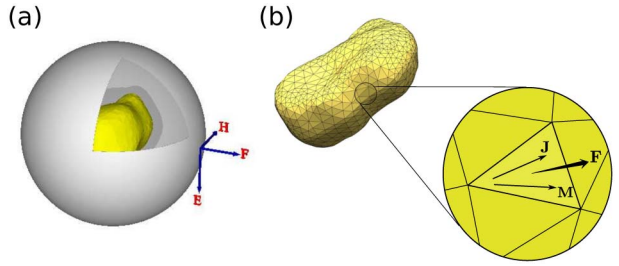

Fig. 1. (a) Traditional approach used to calculate forces on nanostructures requires integrating Maxwell's stress tensor as a function of electric ($\mathbf{E}$) and magnetic ($\mathbf{H}$) fields over a fictitious surface (e.g., a sphere) surrounding the structure; (b) in this Letter, we show that Maxwell's stress tensor can be obtained as a function of surface electric ($\mathbf{J}$) and magnetic ($\mathbf{M}$) currents directly over the surface mesh elements.

$$\mathbf{H} = -\frac{i}{\omega\mu}(\nabla \cdot \mathbf{M})\hat{\mathbf{n}} + \mathbf{J} \times \hat{\mathbf{n}}. \tag{13}$$

Substituting the forms for the surface fields Eq. (12) and Eq. (13), in Eq. (5), we obtain the surface integral equation for the optical force as:

$$\begin{aligned}\mathbf{F} = \sum_T \int_T \mathrm{d}S_T \Bigg\{ & \frac{(\nabla \cdot \mathbf{M})(\nabla \cdot \mathbf{M}^*)}{2\omega^2\mu^*}\hat{\mathbf{n}} + \frac{(\nabla \cdot \mathbf{J})(\nabla \cdot \mathbf{J}^*)}{2\omega^2\epsilon^*}\hat{\mathbf{n}} \\ & + \frac{i}{\omega}\left[\frac{\mu}{\mu^*}(\mathbf{J} \times \hat{\mathbf{n}})(\nabla \cdot \mathbf{M}^*) + \frac{\epsilon}{\epsilon^*}(\hat{\mathbf{n}} \times \mathbf{M})(\nabla \cdot \mathbf{J}^*)\right] \\ & - \frac{1}{2}(\epsilon \mathbf{M} \cdot \mathbf{M}^* + \mu \mathbf{J} \cdot \mathbf{J}^*)\hat{\mathbf{n}}\Bigg\}.\end{aligned} \tag{14}$$

Equation (14) is the main result of this Letter. The SIE expands the surface currents over each triangle in terms of RWG basis functions [26], and the surface currents have the following forms

$$\mathbf{J} = \gamma_1(\mathbf{r} - \mathbf{r_1}) + \gamma_2(\mathbf{r} - \mathbf{r_2}) + \gamma_3(\mathbf{r} - \mathbf{r_3}), \tag{15}$$

$$\mathbf{M} = \delta_1(\mathbf{r} - \mathbf{r_1}) + \delta_2(\mathbf{r} - \mathbf{r_2}) + \delta_3(\mathbf{r} - \mathbf{r_3}), \tag{16}$$

where $\mathbf{r}_i$ is the vertices of the triangle, and γ_i and δ_i are the coefficients associated with each vertex. After substituting Eq. (15) and Eq. (16) in Eq. (14), the integrals can be calculated analytically. The integral of the tensor over each triangle can be expressed in terms of just the polynomial powers of position over the triangle, and can thus be computed in $O(1)$ time. Hence, once the currents are known, the force calculation takes $O(N)$ time only, where N is the number of triangles the surface is discretized into. In comparison, had we created an imaginary surface surrounding the structure and evaluated fields on K points on it, the field evaluation step would have had a time complexity of $O(NK)$. Note that there is also a factor associated with the computation of Green's tensor in the latter case, which can become quite significant if the background is complex and the Green's tensor evaluation is costly.

To demonstrate the validity of the technique, we compare our numerical results with the exact solution given by the Mie theory. The force on a silver sphere of a 30 nm radius when illuminated by a linearly polarized plane wave at $\lambda = 390$ nm is computed. Since we obtain the force on every mesh describing the surface of the object, we can also compute the torque. This is done for the same geometry, but the sphere is now illuminated with a circularly polarized plane wave at the same wavelength. The dielectric constant of the sphere is taken from Johnson and Christy [27]. The variation of the error with the discretization of the spherical surface is shown in Fig. 2. It is evident from the results that the error can be sufficiently minimized with suitable discretization of the structure.

After having demonstrated the accuracy of the method, we investigate a compound plasmonic system consisting of two spheres separated by a distance d [15,28,29]. For the simulation, we consider two silver spheres of 30 nm radius separated by a center to center

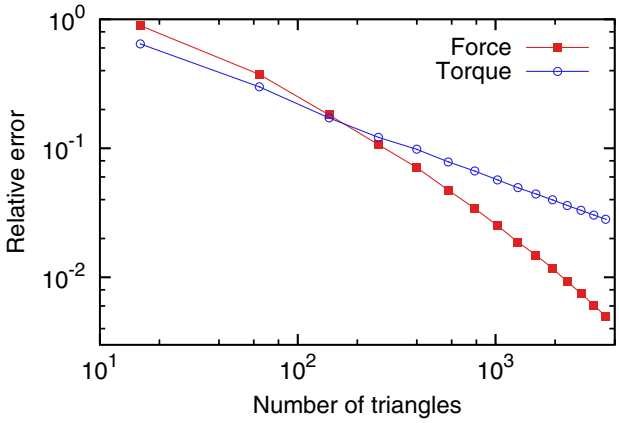

Fig. 2. Relative error in force (**F**) and torque (**T**) as a function of the number of triangles the surface is discretized into for a sphere of 30 nm radius illuminated at $\lambda = 390$ nm.

distance of $d = 70$ nm and 80 nm. The wavelength dependence of the force for both separations is plotted in Fig. 3. The force between the particles is attractive for the entire wavelength range. We clearly see the signature of plasmonic resonance in the present system. The resonance blue shifts as the gap between the spheres is increased. The z component of the force F_z shows similar magnitudes at the plasmon resonances for both separations since z is the direction of the incident wave. Hence, the force in the z direction is primarily the radiation force and is not affected significantly by the interaction with the other sphere, Fig. 3(a). However, the x component of the force is the internal force between the two spheres arising from the electromagnetic interaction between them. Therefore increasing the distance between the spheres reduces the x component of the force F_x, as expected.

We now examine the effect of distance between the spheres more thoroughly. Figure 4 shows the variation of the force between the nanoparticles for a given incident wavelength $\lambda = 370$ nm as the separation is varied from 100 to 900 nm. The z component of the force F_z saturates to a constant value as the distance between them is increased. As explained earlier, this is the expected behavior since this is the radiation force. On the other hand, the x component of the force F_x oscillates in magnitude. This can be understood as follows. The incident field induces dipole moments in both spheres which are very similar in magnitude and phase. The force between two identical dipoles oscillates between attractive and repulsive depending on the separation between them because of retardation effects [30]. Moreover, the forces on the two spheres are equal and opposite because of the symmetry of the system, which again confirms the numerical validity and accuracy of our formalism, Fig. 4(b).

Finally, we extend our formalism to calculate the torque on a realistic structure with a very complex surface geometry shown in the inset of Fig. 5. The structure

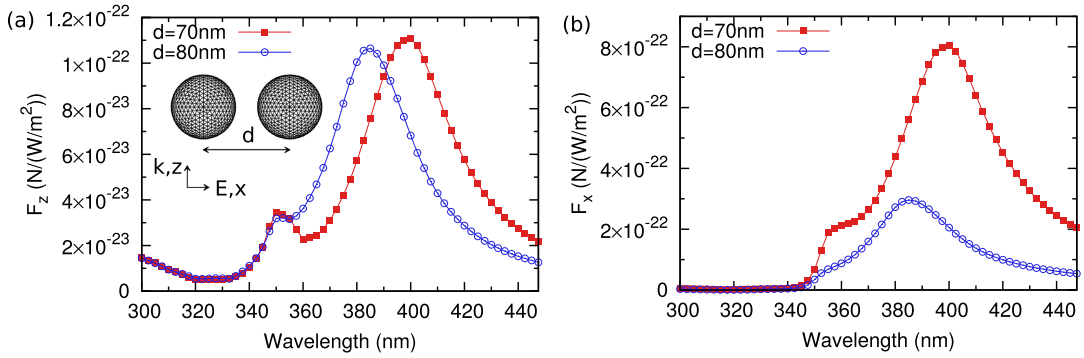

Fig. 3. Wavelength dependence of (a) z component, and (b) x component of optical force on one sphere of a two-sphere system composed of two silver spheres of 30 nm radius separated by a center to center distance of d. The system is illuminated by a plane wave incident along z and polarized along x, as illustrated in the inset of panel (a), and the force is computed for the sphere on the left.

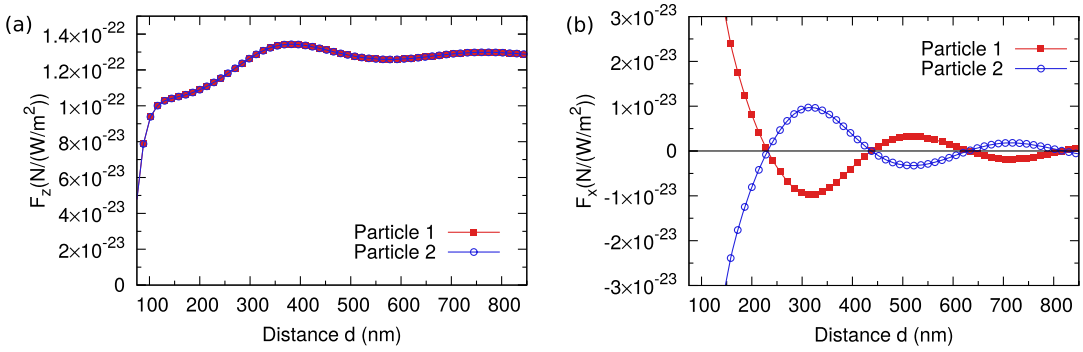

Fig. 4. Distance dependence of (a) z component, and (b) x component of optical force on each sphere of a two-sphere system composed of two silver spheres of 30 nm radius separated by a center to center distance of d. The illumination geometry is the same as that in the inset of Fig. 3(a), and the wavelength of the incident light is $\lambda = 370$ nm. Particle 1 is the sphere on the left.

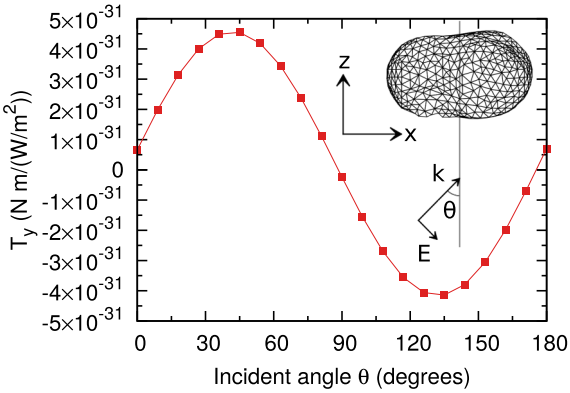

Fig. 5. Dependence of the y-component of torque (T_y) on the angle of incidence (θ) for the realistic structure shown in the inset for TM-polarized plane wave illumination at $\lambda = 500$ nm.

has approximate dimensions of 50 nm × 30 nm × 30 nm, and is illuminated by a TM-polarized plane wave in the xz plane, incident at an angle θ with the z axis. The y component of torque is plotted as a function of the angle of incidence in Fig. 5 and shows significant changes. When the incident wave is normal to the principal axes of the system, the torque is small in magnitude. The magnitude increases for oblique incidence. Such torque calculation as done here can be used for understanding the motion of asymmetric particles in a optical tweezer.

To summarize, we have developed a novel formalism for the calculation of optical forces and torques on realistically shaped scatterers including plasmonic structures using SIE formulation and Maxwell's stress tensor. The method is straightforward, flexible and bypasses some numerical steps to give highly accurate results. In particular, the complete calculation including optical forces and torques on an arbitrarily shaped object only requires the discretization of the object surface. (Note however that the associated SIE matrix is full.) We have applied this formalism to some simple as well as complicated systems to prove its validity and accuracy by comparing it to existing calculations.

Funding from the Swiss National Science Foundation (Project 200020_135452) and from the EPFL International Relations Office is gratefully acknowledged.

†Both authors contributed equally.

References

1. D. G. Grier, Nature **424**, 810 (2003).
2. K. C. Neuman and S. M. Block, Rev. Sci. Instrum. **75**, 2787 (2004).
3. J. R. Moffitt, Y. R. Chemla, S. B. Smith, and C. Bustamante, Annu. Rev. Biochem. **77**, 205 (2008).
4. M. Righini, A. S. Zelenina, C. Girard, and R. Quidant, Nat. Phys. **3**, 477 (2007).
5. A. Grigorenko, N. Roberts, M. Dickinson, and Y. Zhang, Nat. Photonics **2**, 365 (2008).
6. L. Huang and O. J. F. Martin, Opt. Lett. **33**, 3001 (2008).
7. L. Huang, S. J. Maerkl, and O. J. F. Martin, Opt. Express **17**, 6018 (2009).
8. W. Zhang, L. Huang, C. Santschi, and O. J. F. Martin, Nano Lett. **10**, 1006 (2010).
9. M. L. Juan, M. Righini, and R. Quidant, Nat. Photonics **5**, 349 (2011).
10. S. Lin, W. Zhu, Y. Jin, and K. B. Crozier, Nano Lett. **13**, 559 (2013).
11. C. Girard, A. Dereux, and O. J. F. Martin, Phys. Rev. B **49**, 13872 (1994).
12. P. C. Chaumet and M. Nieto-Vesperinas, Phys. Rev. B **61**, 14119 (2000).
13. M. Nieto-Vesperinas, P. C. Chaumet, and A. Rahmani, Phil. Trans. R. Soc. London A **362**, 719 (2004).
14. M. Mazilu, A. Rudhall, E. M. Wright, and K. Dholakia, J. Phys. Condens. Matter **24**, 464117 (2012).
15. A. J. Hallock, P. L. Redmond, and L. E. Brus, Proc. Natl. Acad. Sci. USA **102**, 1280 (2005).
16. A. Salandrino, S. Fardad, and D. N. Christodoulides, J. Opt. Soc. Am. B **29**, 855 (2012).
17. M. Fujii, Opt. Express **18**, 27731 (2010).
18. M. Mansuripur, Nat. Photonics **7**, 765 (2013).
19. J. D. Jackson, *Classical Electrodynamics* (Wiley, 1998).
20. M. Ploschner, M. Mazilu, T. F. Krauss, and K. Dholakia, J. Nanophoton. **4**, 041570 (2010).
21. A. Lovera and O. J. F. Martin, Appl. Phys. Lett. **99**, 151104 (2011).
22. F. J. García de Abajo and A. Howie, Phys. Rev. B **65**, 115418 (2002).
23. U. Hohenester and J. Krenn, Phys. Rev. B **72**, 195429 (2005).
24. A. M. Kern and O. J. F. Martin, J. Opt. Soc. Am. A **26**, 732 (2009).
25. B. Gallinet, A. M. Kern, and O. J. F. Martin, J. Opt. Soc. Am. A **27**, 2261 (2010).
26. S. Rao, D. Wilton, and A. Glisson, IEEE Trans. Antennas Propag. **30**, 409 (1982).
27. P. B. Johnson and R. W. Christy, Phys. Rev. B **6**, 4370 (1972).
28. Z. Li, M. Käll, and H. Xu, Phys. Rev. B **77**, 085412 (2008).
29. V. D. Miljković, T. Pakizeh, B. Sepulveda, P. Johansson, and M. Käll, J. Phys. Chem. C **114**, 7472 (2010).
30. É. Lamothe, G. Lévêque, and O. J. F. Martin, Opt. Express **15**, 9631 (2007).